This article has been accepted for publication in a future issue of this journal, but has not been fully edited. Content may change prior to final publication. Citation information: DOI 10.1109/ACCESS.2020.3024251, IEEE Access

Date of publication xxxx 00, 0000, date of current version xxxx 00, 0000.

Digital Object Identifier 10.1109/ACCESS.2017.DOI

Brake Fault Identification and Fault-Tolerant Directional Stability Control of Heavy Road Vehicles

RADHIKA RAVEENDRAN[1], K. B. DEVIKA[2], SHANKAR C. SUBRAMANIAN.[3], (Senior Member, IEEE)

[1]Research Scholar, Department of Engineering Design, IIT Madras, Chennai, India. (e-mail: radhikaraveendran@gmail.com).
[2]Post Doctoral Fellow, Department of Engineering Design, IIT Madras, Chennai, India. (e-mail: devikakb@gmail.com).
[3]Professor and V. Ramamurti Faculty Fellow, Department of Engineering Design, IIT Madras, Chennai 600 036, India. (e-mail: shankarram@iitm.ac.in).

Corresponding author: Shankar C. Subramanian (e-mail: shankarram@iitm.ac.in).

Research supported by the Ministry of Skill Development and Entrepreneurship, Government of India, through the grant EDD/14-15/023/MOLE/NILE.

ABSTRACT Accurate fault diagnosis in air brake is crucial to reduce frequent brake inspection and maintenance in heavy commercial road vehicles. Existing model-based fault diagnostic schemes work well under limited vehicle operating conditions, which is insufficient for developing an on-board monitoring device. In this context, a learning-based fault identification scheme using the Random Forest technique, which accommodates the vehicle's wide operating conditions, is proposed. This scheme identifies the brake's fault levels with a better classification accuracy of 92% compared to techniques such as Naïve Bayes, k-Nearest Neighbors, Support Vector Machine, and Decision Tree. Further, a fault-tolerant controller is proposed to overcome the vehicle's directional instability arising due to the brake fault. Two sliding mode controllers, namely differential brake control and steering angle control, were developed to control the yaw angle. These have been implemented in a Hardware in Loop experimental platform with the vehicle dynamic simulation software TruckMaker®.

INDEX TERMS Classification algorithms, Fault diagnosis, Fault-tolerant controller, Heavy Road Vehicle, Machine Learning, Random forests, Sliding mode controller, Supervised learning

I. INTRODUCTION

HEAVY Commercial Road Vehicles (HCRVs) use air brake systems, whose failure leads to the vehicle's yaw instability and increased stopping distance. The excessive stroke length of a component called pushrod is one of the major faults in the air brake system. The increase in clearance between the brake lining and the brake drum is due to worn out brake lining and thermal expansion of brake drum, which causes excessive stroke length [1]. However, the maintenance or repair of brakes cannot always be achieved immediately. It requires a human being to go underneath the vehicle to measure/observe the pushrod stroke manually. Further, this approach is time-consuming and becomes difficult for vehicles with low ground clearance. Active safety systems such as ABS, traction control, and electronic stability control require a properly functioning brake system, as it is the primary actuator in the control loop. HCRVs with an active safety system should be fault-tolerant in ensuring the vehicle's stability and delivering the expected vehicle performance. Hence, a Fault-Tolerant Controller (FTC) capable of guaranteeing the vehicle's stability during brake failures is essential.

The design of the FTC system requires an accurate and tractable diagnostic scheme for decision making. For preserving the safety of human occupants and reliability of vehicle operations, the occurrence of faults must be taken into account to generate a fault flag, which would trigger the FTC. Existing fault diagnostic schemes for the air brake system have predominantly followed model-based approaches. Kandt *et al*. [2] developed a mathematical model of the air brake system to find the brake stroke from the brake chamber pressure. Subramanian *et al*. [1] developed model-based diagnostic schemes to detect leaks and estimate the pushrod stroke. In [3], the authors developed a model-based diagnostic scheme to predict the out-of-adjustment of the pushrod and the severity of leak in the air brake system. All the methods mentioned above were developed only for a specific set of vehicle operating conditions like low and medium brake applications. Additionally, they require pres-

This article has been accepted for publication in a future issue of this journal, but has not been fully edited. Content may change prior to final publication. Citation information: DOI 10.1109/ACCESS.2020.3024251, IEEE Access

sure sensors that are not economically viable during real-time implementation. Hence, this paper's primary objective is to develop a fault diagnostic model using a machine learning approach, which incorporates the entire range of vehicle operating conditions and uses the readily available wheel speed data to avoid the necessity of additional pressure sensors.

Another vital fact to be noted is that the Anti-lock Brake System (ABS) is mandatory in HCRVs in many countries, including India, U.S.A., Australia, and Brazil [4]–[7]. As the wheel speed sensor is an essential component of ABS, the wheel speed sensor data is readily available in HCRVs. Motivated by these, a fault identification model using the wheel speed sensor data is proposed in this study, which uses a Machine Learning (ML) based multiclass classifier. Various ML algorithms like Naïve Bayes (NB), *k*-Nearest Neighbors (*k*-NN), Support Vector Machine (SVM), Decision Tree (DT), and Random Forest (RF) were compared to obtain the best prediction algorithm.

The ultimate aim of multiclass classification is to distinguish the various class labels of new instances with known attribute values and unknown class labels, which can then be used to make intelligent decisions. The NB algorithm is widely used for classification and is a probabilistic classifier. An application of the NB algorithm in fault diagnosis of vehicle fleet tracking modules can be found in [8]. Another commonly used classification algorithm is *k*-NN, which classifies an object based on distance from its neighbors [9]. Even though *k*-NN is a simple algorithm, its prediction accuracy depends on the distance metric used to calculate the distance between an object and its neighbors. Sankavaram *et al*. developed a fault diagnostic model based on the *k*-NN algorithm in a hybrid electric vehicle regenerative braking system [10]. The DT algorithm is a widely used multiclass classification tool that finds application in many real-world classification problems such as fault diagnosis, weather prediction, and astronomy. Huang *et al*. developed a DT based fault diagnostic model for a fuel cell engine [11]. The issues related to the construction of DTs are the tree's growth to enable it to accurately classify the training data sets and the pruning stage in which unnecessary nodes and branches are removed for better classification accuracy. The disadvantages of DTs can be overcome by the RF algorithm, an ensemble algorithm made of many decision trees using random subsets of features, bootstrapping, and average voting to make predictions [12]. The work in [13] discusses the fault diagnosis of automotive systems based on the RF algorithm. In the present work, fault identification models based on all the ML methods mentioned above have been developed. The various performance measures of these models were compared to obtain the most accurate fault identification scheme. Thus, one of the objectives of this paper is to identify the fault (using a suitable ML model) in the air brake system in the early stage of its occurrence using wheel speed sensor data, which ultimately gives an idea about the severity of the fault. Hence, this would be suitably integrated for advanced vehicle safety systems and intelligent vehicles.

On detecting a faulty brake during the vehicle's operation, the driver should take necessary action to correct any trajectory error through steering command. But the driver's reaction is affected by individual factors, such as driving experience, gender, and habits [14]–[16]. An improper steering command to improve stability may further worsen the situation. In this context, an FTC capable of maintaining vehicle stability under a faulty brake scenario would be of significant interest. Hence, this paper's second objective is to develop an FTC that maintains the yaw angle at the desired values under the brake fault scenario by giving an appropriate control command. Two controllers, namely Differential Braking Controller (DBC) and Steering Angle Controller (SAC), were considered for the FTC scheme. For a better control action in the presence of faulty brake, DBC and SAC's performance were analyzed based on the vehicle's Stopping Distance (SD) and yaw angle reduction. Here, the proposed methodology works so that, whenever a brake fault is detected, the controller gets activated and provides the necessary control action.

The variables required for implementing the controller are yaw angle, yaw rate, longitudinal, and lateral vehicle speed. However, vehicle longitudinal and lateral speed are not readily available as measurements in practice. Various estimation schemes are available for longitudinal and lateral speed estimation that use extended Kalman filter [17], adaptive Kalman filter [18], and Sliding Mode Observers (SMO) [19]. Although the performance of the above methods is similar, Kalman filter based estimation schemes require a large amount of computation [20]. But SMO avoids massive matrix computation and gives better parameter robustness and is more practically feasible than the Kalman filter [21]. Hence, in this research, an SMO based estimation scheme has been used to estimate vehicle lateral and longitudinal speeds.

The development of fault-tolerant control schemes for air brake systems has not been adequately explored by the research community. A few related works in this domain for other automotive systems are the following. Li *et al*. developed a fuzzy H_∞ controller for active suspension with actuator delay and fault [22]. An observer-based fault-tolerant controller for uncertain steer-by-wire systems using model predictive control has been developed by Haung *et al*. [23]. A nonlinear fault-tolerant control scheme has been developed by Youssef *et al*. considering vehicle lateral dynamics using T-S fuzzy model [24]. Chen *et al*. designed a sliding mode control based FTC considering a hypersonic flight vehicle's longitudinal dynamics [25]. Guo *et al*. developed a sliding mode FTC for nonlinear systems with actuator fault [26].

A nonlinear vehicle model suitable for scenarios like combined braking and cornering has been used in this study. Further, the control technique for FTC should have adequate robustness to tolerate the incidence of potential parametric uncertainties and external disturbances during on-road vehicle operation. In this regard, due to its suitability for nonlinear systems, and also by virtue of its robustness, Sliding Mode Control (SMC) has been used in this study for

FTC design [27], [28]. SMC is a well established control technique for various control engineering problems [29]. Chae *et al*. developed a dynamic handling control scheme for electric vehicles using adaptive SMC [30]. An adaptive SMC scheme was designed to eliminate the thruster faults and external disturbances for a spacecraft by Liu et al. [31]. Anche *et al.* developed a hitch control system to attenuate the disturbance forces in tractors [32]. In order to overcome the inherent limitation of chattering in SMC (high-frequency control signal switching), a reaching law based SMC design has been employed for FTC design [33].

Based on related literature, it was observed that a proper diagnostic tool, along with an adequate FTC scheme for the air brake system, is not available. In view of this, a diagnostic method that considers the vehicle's wide operating conditions and an FTC scheme that preserves the vehicle's stability in the event of brake system failure has been presented in this paper. The key features of this study are:

- Design of experiments is proposed for the collection of extensive data sets required for the development of fault identification models.
- Various multiclass algorithms for fault identification of the air brake system using the wheel speed sensor data are developed and compared.
- An SMO based observer is designed for estimating the vehicle longitudinal and lateral speed that are essential for FTC design.
- In order to maintain vehicle directional stability under the brake fault scenario, an SMC based FTC is designed and implemented in a Hardware-in-Loop (HiL) experimental platform.

The rest of this article is organized as follows. Section II deals with the theoretical background of fault identification schemes. The overview of fault-tolerant control, along with fault identification structure, is discussed in section III. The experimental setup and the data collection procedure are explained in section IV. Section V discusses the fault identification of the air brake system using multiclass classifiers. Section VI explains the FTC design and analysis, including the description of the vehicle model, SMO design and controller design, and its performance evaluation. Finally, section VII concludes the paper.

II. FAULT IDENTIFICATION METHODS

Fault detection and diagnosis consist of three steps, namely fault detection, isolation, and identification. The present study deals with fault identification of the Front Right (FR) brake system using various ML techniques viz., Naïve Bayes (NB), *k*-Nearest Neighbors (*k*-NN), Decision Tree (DT), Support Vector Machines (SVMs) and Random Forest (RF). These methods are briefly discussed below.

1) Naïve Bayes Algorithm

The Naïve Bayes (NB) classifier technique is based on the Bayes theorem and is capable of handling an arbitrary number of independent variables. As per the Bayes theorem,

$$p(a_j|b) = \frac{p(b|a_j)p(a_j)}{p(b)}, \tag{1}$$

where, $p(a_j|b)$ is the probability of instance b in class a_j, $p(b|a_j)$ is the probability of generating instance b given class a_j, $p(a_j)$ is the probability of occurrence of class a_j, and $p(b)$ is the probability of occurrence of instance b. The Naïve Bayes classifier assumes independence among attributes for a given class [34].

2) k-Nearest Neighbor Algorithm

In the *k*-Nearest Neighbor (*k*-NN) algorithm, the classification of an object is obtained based on distance from its neighbors. The commonly used method of measuring distance is the Euclidean distance metric method. Here, the *k*-NN algorithm selects only the *k*-nearest neighbor classes based on a majority vote that would predict the best-fit class for a point [9].

3) Decision Tree Algorithm

Decision tree (DT) builds classification algorithms in the form of a tree structure and uses a set of binary rules to calculate a target value. It consists of a root node, which represents the entire samples, each internal node corresponds to a "test" on an attribute, and finally, each leaf gives a class label. The basic algorithm used in DT is known as the Iterative Dichotomiser 3 (ID3) algorithm, which develops decision trees using a top-down approach [35].

4) Random Forest Algorithm

Random Forest (RF) algorithm is an ensemble based algorithm, which consists of several decision trees. The two key concepts in the RF algorithm are the random sampling of training data points for building trees and random subsets of features for splitting nodes [12], [36]. One of the main advantages of using the RF algorithm is that it is free from the model overfitting issues. In the present study, the number of trees used in the forest was 50, the minimum number of samples required to split an internal leaf node was taken as 2, and the minimum number of samples required at a leaf node was taken as 1.

5) Support Vector Machines (SVMs)

SVMs are designed for binary classification, which gives an outcome of +1 or -1 [37]. But at the same time, it is an excellent tool for multiclass classification. Two different approaches are mainly considered for a multiclass SVM: one-against-all (OAA) and one-against-one (OAO). OAA uses *K* binary problems to classify *K* classes in which each problem discriminates a given class from the other (*K*-1) classes. For this approach, the system requires *K* binary classifiers. In OAO, each classifier is trained to distinguish between each pair of classes. This design exhausts all combinations of positive class assignments. Hence, this approach requires

This article has been accepted for publication in a future issue of this journal, but has not been fully edited. Content may change prior to final publication. Citation information: DOI 10.1109/ACCESS.2020.3024251, IEEE Access

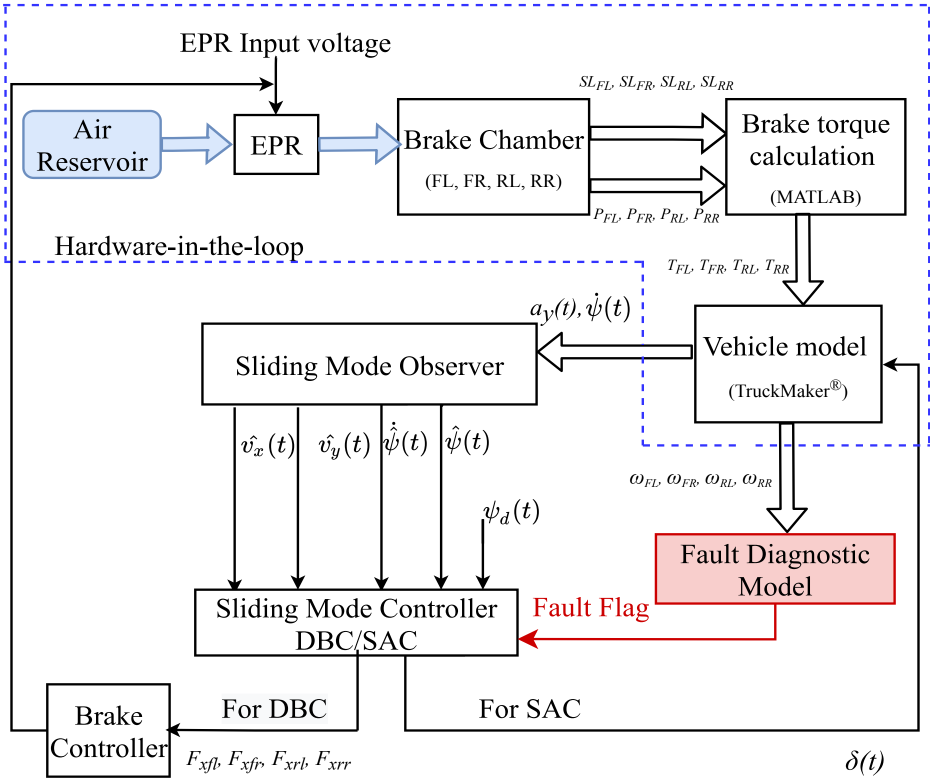

FIGURE 1: Overview of differential braking based and steering angle based Fault Tolerant Controller along with fault identification scheme

$K(K\text{-}1)/2$ binary classifiers [38], [39]. SVM-OAO is typically more accurate than the SVM-OAA [38], and hence, SVM-OAO was used to classify three levels of faults in the air brake system. Here, the SVM parameters were optimized using a 10-fold cross-validation approach. Two kernel techniques, viz., linear and Gaussian kernels were used in the present study.

III. OVERVIEW OF FAULT-TOLERANT CONTROL ALONG WITH FAULT IDENTIFICATION STRUCTURE

Fig. 1 represents the overall block schematic of the proposed FTC scheme based on Differential Braking Control (DBC)/Steering Angle Control (SAC). Here, the Hardware-in-the-Loop (HiL) experimental platform consists of an Electro-Pneumatic Regulator (EPR) based air brake system. Initially, air brake fault was identified by a multiclass ML model. Once the fault flag gets activated, the FTC controller has to give the required control command for vehicle stability. A sliding mode controller design based on conventional constant rate reaching law (CRRL) and power rate exponential reaching law (PRERL) has been developed to implement DBC and SAC. In SAC, the steering angle is the control signal fed back to the vehicle model. On the other hand, in DBC, brake force is the control signal converted to the desired brake pressure and then realized through a brake controller.

IV. EXPERIMENTAL SETUP AND DATA COLLECTION

A. EXPERIMENTAL SETUP

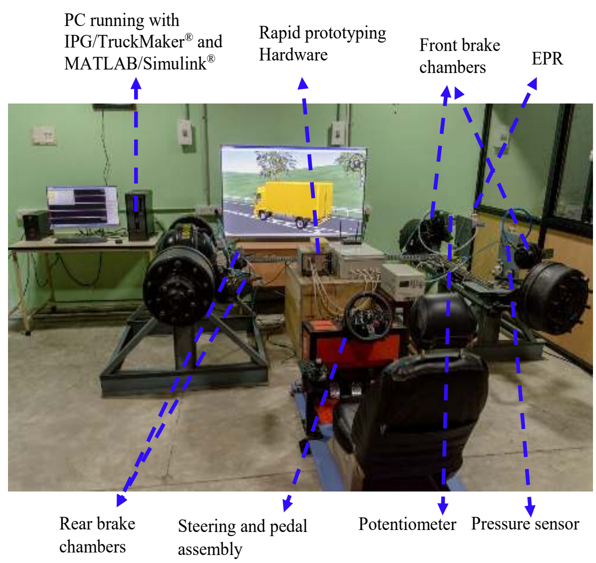

FIGURE 2: Hardware-in-the-loop (HiL) experimental setup of air brake system in HCRVs

This article has been accepted for publication in a future issue of this journal, but has not been fully edited. Content may change prior to final publication. Citation information: DOI 10.1109/ACCESS.2020.3024251, IEEE Access

The Hardware-in-the-Loop (HiL) experimental setup used in the present study (Fig. 2) consists of:

- HCRV brake system along with the vehicle dynamic simulation software IPG/ TruckMaker®.
- Flexible and modular hardware viz., IPG XPack4, which acts as a Real-Time Rapid Control Prototyping tool.
- Pressure sensors for measuring brake chamber pressure.
- Electro-Pneumatic Regulators (EPRs), used to regulate the pressure, allow the compressed air from the storage reservoir to the brake chamber based on an analog DC voltage supplied between 0-10 V.
- Potentiometers interfaced with the control hardware for measuring the pushrod stroke.

B. VEHICLE PARAMETERS

TABLE 1: Vehicle parameters [40]

Parameter	Unladen vehicle Values	Laden vehicle Values
Mass, M	4700 kg	16200 kg
Distance from Front Axle, L_f	2.7 m	3.4 m
Distance from Rear Axle, L_r	2.7 m	2.0 m
CG Height, h	1 m	1.3 m
Moment of Inertia (X-axis), I_x	6176 kgm^2	20000 kgm^2
Moment of Inertia (Z-axis), I_z	39000 kgm^2	100000 kgm^2
Cornering stiffness, $C_{\alpha f}$	79322 N/rad	330683 N/rad
Cornering stiffness, $C_{\alpha r}$	82748 N/rad	186589 N/rad
Track Width, d	2.1 m	2.1 m

A 16200 kg truck was used in this study [40]. A wheelbase of 5.4 m and a straight line maneuver with an initial longitudinal speed of 80 km/h (22.22 m/s) were considered. The brake was applied for a duration of 10 s. The vehicle parameters used in the current analysis are given in Table 1.

C. DATA COLLECTION PROCEDURE

The feature set for developing the ML model consists of wheel speed data from the four wheels. Fig. 3 shows the test scenarios used for the data collection. Data sets corresponding to broad combinations of physical parameters (e.g. vehicle load, brake and road conditions) representing realistic vehicle operating conditions were considered in order to achieve good prediction accuracy. Thus, vehicle load conditions (fully laden and fully unladen), various brake chamber pressures from 0.1 MPa to 0.9 MPa with a step size of 0.1 MPa, tire-road interface friction values ($\mu_{\max} = 0.8$, $\mu_{\max} = 0.3$ and split μ) and brake conditions (No-fault, 10%, and 20% brake torque reduction) were the test scenarios considered for the collection of training data sets. In order to illustrate the efficacy of the developed ML models, partially laden (50% of maximum load), random pressure application,

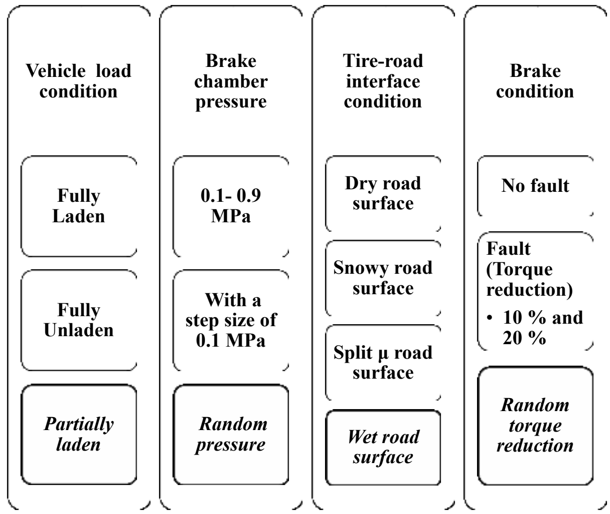

FIGURE 3: Various vehicle operating and road conditions for collecting training (normal font) and testing data (both normal font and italics font)

tire-road interface friction value $\mu_{\max} = 0.5$ and random torque reductions were also included in the testing process.

Since the wheel speed sensor data is highly sensitive to the various vehicle operating conditions and working conditions of all four brakes, a detailed test matrix was designed by encompassing the four test scenarios (Fig. 3) and is shown in Table 2. The proposed scheme for fault identification is intended to develop diagnostic algorithms separately for all the four brakes. For the sake of brevity, this paper demonstrates the fault diagnostic algorithm for the front right brake alone.

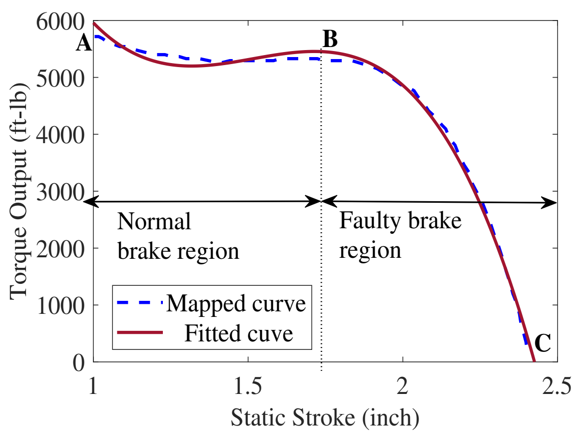

FIGURE 4: Brake torque variation with static pushrod stroke length [41]

In order to obtain the various fault levels for fault identification, the vehicle performance analysis has been conducted in terms of the yaw angle deviation and stopping distance. The relation between brake torque and the pushrod stroke length is shown in Fig. 4, and it is clear that the brake

This article has been accepted for publication in a future issue of this journal, but has not been fully edited. Content may change prior to final publication. Citation information: DOI 10.1109/ACCESS.2020.3024251, IEEE Access

TABLE 2: Test matrix for fault identification of front right brake chamber

Test Case	Fault level	Front right	Front left	Rear right	Rear left	Fault Identification label	No.of Training data
Case I	No fault	NF	NF	NF	NF	FRNF	54
	10% fault	F	NF	NF	NF	FRF10%	54
	20% fault	F	NF	NF	NF	FRF20%	54
Case II	No fault	NF	F	NF	NF	FRNF	54
	10% fault	F	F	NF	NF	FRF10%	54
	20% fault	F	F	NF	NF	FRF20%	54
Case III	No fault	NF	NF	F	NF	FRNF	54
	10% fault	F	NF	F	NF	FRF10%	54
	20% fault	F	NF	F	NF	FRF20%	54
Case IV	No fault	NF	NF	NF	F	FRNF	54
	10% fault	F	NF	NF	F	FRF10%	54
	20% fault	F	NF	NF	F	FRF20%	54
Case V	No fault	NF	F	F	NF	FRNF	54
	10% fault	F	F	F	NF	FRF10%	54
	20% fault	F	F	F	NF	FRF20%	54
Case VI	No fault	NF	NF	F	F	FRNF	54
	10% fault	F	NF	F	F	FRF10%	54
	20% fault	F	NF	F	F	FRF20%	54
Case VII	No fault	NF	F	NF	F	FRNF	54
	10% fault	F	F	NF	F	FRF10%	54
	20% fault	F	F	NF	F	FRF20%	54
Case VIII	No fault	NF	F	F	F	FRNF	54
	10% fault	F	F	F	F	FRF10%	54
	20% fault	F	F	F	F	FRF20%	54
Total training data							**1296**

torque drastically reduces after a particular stroke length (readjustment limit). The reduction of brake torque in any brake chamber affects vehicle performance (yaw stability and stopping distance), and it becomes more severe under varying tire-road interface conditions and load conditions of the vehicle. The variation of yaw angle and stopping distance corresponding to different levels of brake torque reduction in the front right brake of a fully laden vehicle with $\mu_{max} = 0.8$ and brake pressure of 0.8 MPa is shown in Fig. 5.

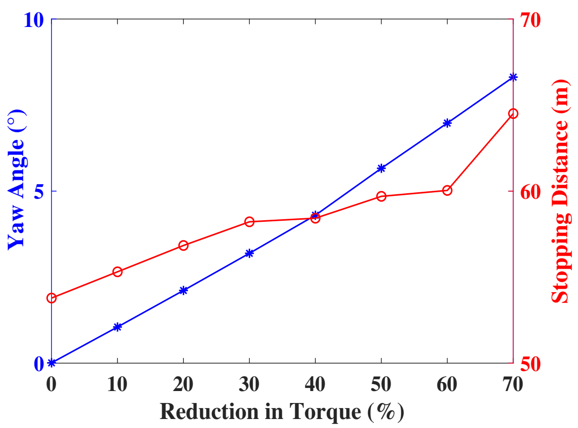

FIGURE 5: Yaw angle and stopping distance corresponding to the different level of brake torque reduction in front right brake

The effect of stopping distance and yaw angle variations with a reduction in brake torque was analyzed for a vehicle with a length of 8.1 m and a width of 2.1 m on a road with a lane width of 3.5 m. The yaw angle at 20% and 30% reduction in brake torque was found to be 2^o and 3^o, respectively, and it was observed that at 30% brake torque reduction, the vehicle would go outside the lane boundary. Similarly, the corresponding increase in stopping distance was found to be 3.6 m and 4.6 m, respectively. Hence, it is clear that a 30% torque reduction is a severe fault and the performance would not deteriorate much at 20% torque reduction. Hence, it was determined that it is essential to detect the fault when it reaches a level of at most 20%. From this analysis, the fault levels of front right brake were fixed as FRNF, FRF10%, and FRF20% corresponding to no-fault, 10% torque reduction, and 20% torque reduction, respectively. The labels FRF and FRNF correspond to the front right faulty brake and front right non-faulty brake, respectively. For developing fault diagnosis algorithms for other brakes, Table 2 can be relabelled accordingly.

Data sets were collected by conducting 1795 test runs that include 1296 training data sets and 499 testing data sets. Each wheel speed data consists of 1000 data points collected at a sampling rate of 50 Hz.

V. FAULT IDENTIFICATION USING MACHINE LEARNING TECHNIQUES

A. PERFORMANCE ANALYSIS OF VARIOUS ML TECHNIQUES

For fault identification, the multiclass algorithm is required to classify at least three classes of fault levels. Here, the

This article has been accepted for publication in a future issue of this journal, but has not been fully edited. Content may change prior to final publication. Citation information: DOI 10.1109/ACCESS.2020.3024251, IEEE Access

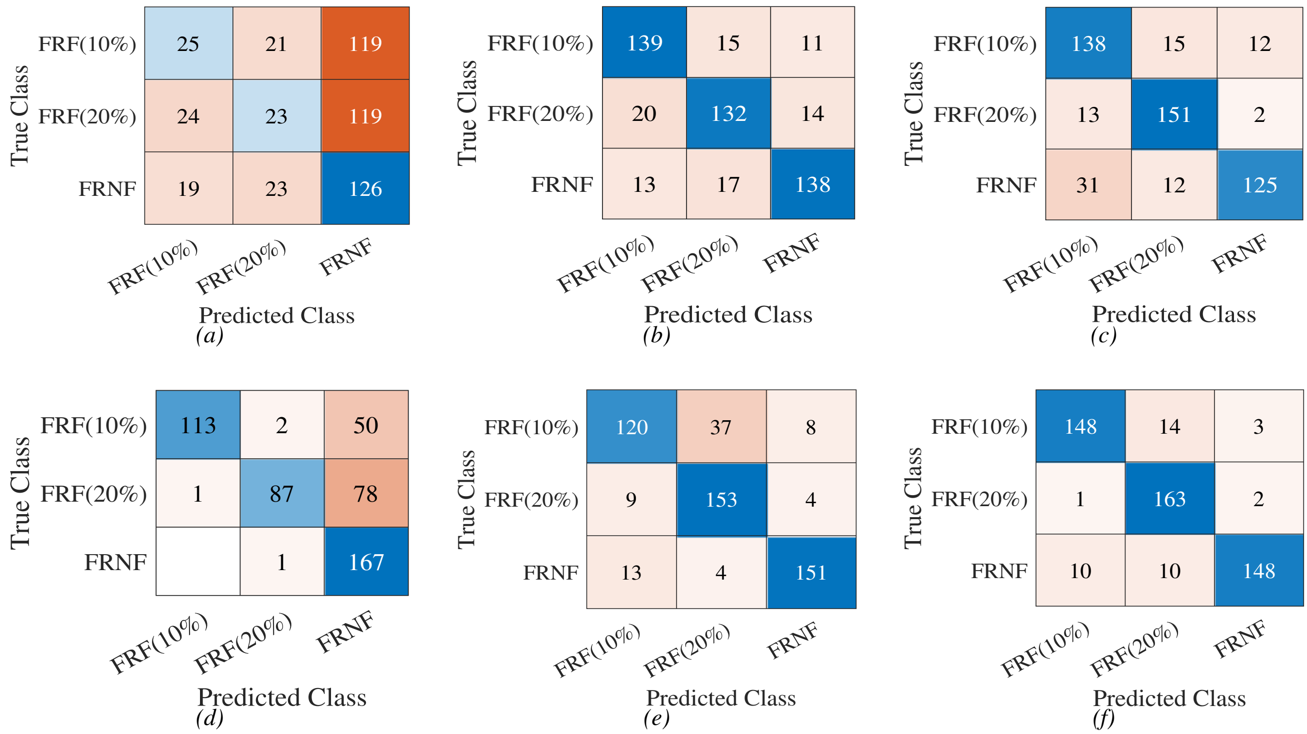

FIGURE 6: Confusion matrix for fault level classification of air brake system based on wheel speed sensor data: (a) Naïve Bayes, (b) *k*-Nearest Neighbor, (c) Decision Tree, (d) SVM (Linear), (e) SVM (Gaussian), (f) Random Forest

TABLE 3: Performance measures of various ML techniques

Performance Measures	**Random Forest**			**SVM (Gaussian)**			**SVM (Linear)**			**Decision Tree**			***k*-Nearest Neighbor**			**Naïve Bayes**		
	C1	C2	C3	C1	C2	C3	C1	C2	C3	C1	C2	C3	C1	C2	C3	C1	C2	C3
Precision (%)	88	98	89	89.9	92.2	72	99	52	68	74	91	83	82	79	84	75	14	15
Recall (%)	96.7	87.2	93	92	79	85	56	97	99	90	85	76	85	81	81	35	34	37
Class Accuracy (%)	**97**	**95**	**94**	94	89	86	74	81	87	88	91	85	88	86	87	38	48	49
Average Accuracy (%)	**94.51**			89.55			81.4			88.02			87.21			45.09		
Overall Accuracy (%)	**91.99**			84.97			73.54			82.97			81.96			34.87		
Computation Time (s)	**0.33**			2.22			0.345			0.213			1.08			0.415		

$\mathbf{C1} \Rightarrow Class1 : FRNF, \mathbf{C2} \Rightarrow Class2 : FRF(20\%), \mathbf{C3} \Rightarrow Class3 : FRF(10\%)$

fault levels were taken as No-Fault, 10%, and 20% fault on the front right brake with corresponding labels FRNF, FRF (10%), and FRF (20%), respectively. The developed models were tested with 499 data sets that include random operating conditions of vehicle load and road scenarios. The confusion matrix corresponding to various ML models is given in Fig. 6. Here, the diagonal entry of the confusion matrix shows the number of correct classifications and the off-diagonal entry represents the wrong classifications. The performance measures like precision, recall, and accuracy of the various ML models are given in Table 3. Here, class accuracy, average accuracy (average of each accuracy per class), and overall accuracy (number of correctly predicted items/total of the item to predict) were calculated for all ML models. The average and overall accuracy of the RF model were 94.51% and 91.99%, respectively, which is the highest performance compared to the other ML models. It was noted that, with an Intel Core^{TM} Processor i5-6200U CPU with 8GB RAM, the computation time for testing with a single set of data was 0.33 s in the case of the RF model. Based on this analysis, it can be concluded that the Random Forest model provided the best prediction accuracy for correct classification of various fault levels of the air brake system.

VI. FAULT TOLERANT CONTROL SCHEME DESIGN AND ANALYSIS

A. THE VEHICLE MODEL

The current study used a two track vehicle model with 3 degrees of freedom (3 DOF) (longitudinal, lateral, and yaw motion of the vehicle), which is shown in Fig. 7. The pitch and roll motions have been neglected. Here, δ is the front wheel steering angle, l_f and l_r denote, respectively, the distance of center of gravity (CG) from the front and rear axle center, d is the track width, F_x denotes the braking force, and the subscripts *fl*, *fr*, *rl*, and *rr* represent, respectively, the front left, front right, rear left and rear right. M is mass of the vehicle, $C_{\alpha f}$, $C_{\alpha r}$ are the cornering stiffness of each front tire and rear tire, respectively. $v_x(t)$ and $v_y(t)$ are the longitudinal and lateral speed of the vehicle, respectively. I_z is the moment of inertia about the z-axis and $\delta(t)$ is the vehicle steering angle. The equations of motion are given by

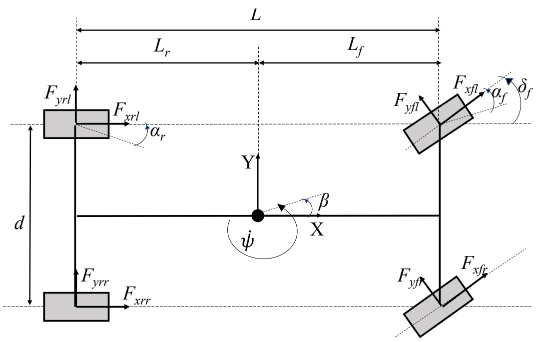

FIGURE 7: Two-track model of a vehicle performing a left turn

$$\dot{v}_x(t) = \dot{\psi}(t)v_y(t) - \frac{C_{\alpha f}}{M}\left(\delta(t) - \frac{v_y(t)+\dot{\psi}(t)l_f}{v_x(t)}\right)\delta(t) - \frac{1}{M}(F_{xfl}(t)+F_{xfr}(t)+F_{xrl}(t)+F_{xrr}(t)), \tag{2}$$

$$\begin{aligned}\dot{v}_y(t) = &-\dot{\psi}(t)v_x(t) + \frac{C_{\alpha r}}{M}\left(\frac{-v_y(t)+\dot{\psi}(t)l_r}{v_x(t)}\right) \\ &- \frac{C_{\alpha f}}{M}\left(\frac{v_y(t)+\dot{\psi}(t)l_f}{v_x(t)}\right) + \frac{C_{\alpha f}}{M}\delta(t) \\ &+ \frac{\delta(t)}{M}\left(F_{xfl}(t)+F_{xfr}(t)\right),\end{aligned} \tag{3}$$

$$\begin{aligned}\ddot{\psi}(t) = &\frac{l_f}{I_z}C_{\alpha f}\delta(t) - \frac{l_f}{I_z}C_{\alpha f}\left(\frac{-v_y(t)+\dot{\psi}(t)l_f}{v_x(t)}\right) \\ &- \frac{l_r}{I_z}C_{\alpha r}\left(\frac{-v_y(t)+\dot{\psi}(t)l_r}{v_x(t)}\right) \\ &- \frac{d}{2I_z}(F_{xfr}(t)-F_{xfl}(t)) - \frac{d}{2I_z}(F_{xrr}(t)-F_{xrl}(t)).\end{aligned} \tag{4}$$

Equations (2), (3), and (4) are represented in state space form as

$$\dot{\mathbf{x}}(t) = \mathbf{f}(\mathbf{x}(t)) + \mathbf{g}(\mathbf{u}(t)), \tag{5}$$

where, state vector

$$\mathbf{x}(t) = \begin{bmatrix} v_x(t) & v_y(t) & \psi(t) & \dot{\psi}(t) \end{bmatrix}^T,$$

and the input vector

$$\mathbf{u}(t) = \begin{bmatrix} F_{xfl}(t) & F_{xfr}(t) & F_{xrl}(t) & F_{xrr}(t) \end{bmatrix}^T.$$

Here, the output equation is,

$$y(t) = \begin{bmatrix} 0 \\ 0 \\ 1 \\ 0 \end{bmatrix} \cdot \begin{bmatrix} v_x(t) \\ v_y(t) \\ \psi(t) \\ \dot{\psi}(t) \end{bmatrix} = \psi(t). \tag{6}$$

The vehicle model given in (5) and (6) was used for FTC design. The Pacejka Magic Formula 6.1 tire model [42] was used in the present study and it is given by

$$y = Dsin[C(arctan(Bx - E(Bx - arctanBx))], \tag{7}$$

where $Y(X) = y(x) + S_V$ and $x = X + S_H$. Here, Y is the output variable (longitudinal force, lateral force or aligning moment), and X is the input variable (longitudinal slip or slip angle). The tire model parameters B, C, D, and E, represent the stiffness factor, the shape factor, the peak value, and the curvature factor. The parameters S_H and S_V denote the horizontal and vertical shifts of the force-slip curve, respectively. The tire model parameters for the 315/80R22.5 radial truck tire were obtained from the vehicle dynamic simulation software, IPG TruckMaker® [43], and used in this study.

B. SLIDING MODE OBSERVER (SMO) DESIGN

Vehicle parameters like longitudinal and lateral speed are not readily available through measurements. Hence, for implementing FTC, these parameters were estimated using a Sliding Mode Observer (SMO). The structure of SMO is given in Fig. 8. The basic SMO design includes two steps:

- Design of intersection of the sliding surface to restrict the estimation error trajectories to the sliding surface with the desired stable dynamics.
- Determination of the observer gain to drive the estimation error trajectories to the sliding surface and maintain it on the surface for all subsequent time.

For the design of SMO, consider the nonlinear system,

$$\dot{\mathbf{x}}(t) = \mathbf{f}(\mathbf{x}(t), \mathbf{u}(t)), \mathbf{z} = \mathbf{h}_{NL}(\mathbf{x}(t)) \tag{8}$$

This article has been accepted for publication in a future issue of this journal, but has not been fully edited. Content may change prior to final publication. Citation information: DOI 10.1109/ACCESS.2020.3024251, IEEE Access

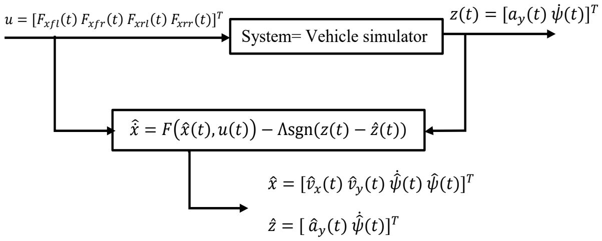

FIGURE 8: Basic structure of Sliding Mode Observer

where,

$$\mathbf{f}(\hat{\mathbf{x}}(t), \mathbf{u}(t)) = \begin{bmatrix} f_1(\hat{\mathbf{x}}(t), \mathbf{u}(t)) \\ f_2(\hat{\mathbf{x}}(t), \mathbf{u}(t)) \\ f_3(\hat{\mathbf{x}}(t), \mathbf{u}(t)) \\ f_4(\hat{\mathbf{x}}(t), \mathbf{u}(t)) \end{bmatrix},$$

$$\mathbf{h}_{NL}(\mathbf{x}(t)) = \begin{bmatrix} h_{NL1}(\mathbf{x}(t)) \\ h_{NL2}(\mathbf{x}(t)) \end{bmatrix},$$

and the measurement vector,

$$\mathbf{z(t)} = \begin{bmatrix} a_y(t) & \dot{\psi}(t) \end{bmatrix}^T.$$

An SMO for the system given in (8) can be designed as

$$\dot{\hat{\mathbf{x}}}(t) = \mathbf{f}(\hat{\mathbf{x}}(t), \mathbf{u}(t)) - \mathbf{\Lambda} \mathbf{z}_s(t), \tag{9}$$

where, $\mathbf{\Lambda}$ is a 4x2 robustness gain matrix and $\mathbf{z}_s(t)$ is 2x1 robustness vector which is expressed by

$$\mathbf{z}_s(t) = \begin{bmatrix} \text{sgn}(\tilde{z}_1(t)) & \text{sgn}(\tilde{z}_2(t)) \end{bmatrix}^T,$$

where,

$$\tilde{z}_1(t) = \hat{a}_y(t) - a_y(t) = s_1(t) \quad \text{and}$$

$$\tilde{z}_2(t) = \dot{\hat{\psi}}(t) - \dot{\psi}(t) = s_2(t).$$

The 2-dimensional surface $\mathbf{s}(t) = [s_1(t) \quad s_2(t)]^T = 0$ will be attractive if outside of the surface there exists

$$s_i(t)\dot{s}_i(t) < 0, \quad i = 1, 2.$$

Further, if

$$s_i(t)\dot{s}_i(t) \le -\eta_i s_i(t), \quad i = 1, 2,$$

holds, system trajectories will reach the surface $s(t) = 0$ in finite time. The above sliding-mode observer has a chattering problem due to the ‘sgn’ discontinuity, which can be eliminated by using a boundary layer approach which uses a ‘saturation’ function instead of ‘sgn’ function [44].

Fig. 9 shows the estimated and actual longitudinal speed and lateral speed during a lane change maneuver for a fully laden vehicle with high tire-road friction coefficient ($\mu_{max} = 0.8$). The efficacy of the algorithm was evaluated with other test maneuvers like steady state circle, braking-in-a-curve and steer step. The performance of SMO was analyzed in terms of Root Mean Square Error (RMSE), and the observations are shown in Table 4. The RMSE of the longitudinal and lateral speed of all cases was less than 0.69 m/s.

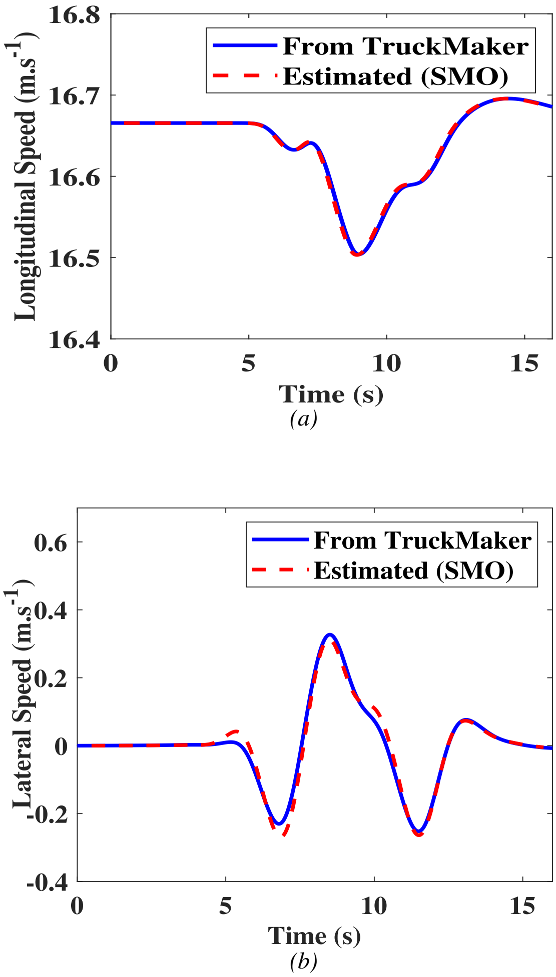

FIGURE 9: Estimated and actual longitudinal speed and lateral speed during a lane change maneuver : a) Longitudinal Speed b) Lateral Speed

TABLE 4: Performance evaluation of SMO based estimation scheme

Test Maneuver	**RMSE** (m/s)	
	Longitudinal Speed	**Lateral Speed**
Lane change	0.02	0.12
Steady State Circle	0.61	0.69
Braking-in-a-curve	0.17	0.42
Steer Step	0.46	0.39

C. CONTROLLER DESIGN USING SLIDING MODE CONTROL

Sliding Mode Control (SMC) is a well accepted robust control technique that finds application in various control engineering problems. SMC is used in this paper to develop a robust FTC for the air brake system. This led to the development of a suitable controller design for maintaining vehicle stability with faulty brakes. Hence, two control actions, namely Differential Braking Control (DBC) and Steering An-

This article has been accepted for publication in a future issue of this journal, but has not been fully edited. Content may change prior to final publication. Citation information: DOI 10.1109/ACCESS.2020.3024251, IEEE Access

gle Control (SAC) were developed, and the performance of the vehicle with both controllers was evaluated. The objective was to regulate the yaw angle (ψ(t)) to zero through adequate:

- Longitudinal brake forces as control inputs in DBC;
- Steering angle as control input in SAC.

Here, the error in state variable is

$$e(t) = x_{3a}(t) - x_{3d}(t) = \psi(t) - \psi_d(t), \tag{10}$$

where, $\psi(t)$ and $\psi_d(t)$ are the actual and desired yaw angle respectively. The desired yaw angle is given by $\psi_d(t)$ and is desired to be 'zero' during a straight line maneuver.

For the design of SMC based controller towards the regulation of the state variable, $\psi(t)$, the switching function was selected as

$$s(t) = \lambda e(t) + \dot{e}(t), \tag{11}$$

where, $\lambda > 0$.
Now taking the first derivative of $s(t)$ and applying the desired values of output variables to zero

$$\dot{s}(t) = \lambda\dot{\psi}(t) + \ddot{\psi}(t). \tag{12}$$

In order to mitigate chattering, reaching law based SMC design has been employed here. The conventional Constant Rate Reaching Law (CRRL) is given by,

$$\dot{s}(t) = -K_c \text{sgn}(s(t)) = \lambda\dot{\psi}(t) + \ddot{\psi}(t). \tag{13}$$

Even though CRRL has been widely used as a simple strategy for SMC design, it introduces chattering in the system. This limits the practical utility of SMC since high frequency control signal switching due to chattering may result in actuator damages [33], [45]. Hence, SMC design should involve adequate chattering mitigation in order to make it suitable for practical application. In this context, the recently proposed Power Rate Exponential Reaching Law (PRERL), which provides chattering mitigation property, has been adopted for air brake system FTC design. The PRERL is given by

$$\begin{aligned}\dot{s}(t) = \frac{-K_p}{\delta_0 + (1-\delta_0)e^{-\alpha|s(t)|^p}}\, |s(t)|^q\, \text{sgn}(s(t)) \\ = \lambda\dot{\psi}(t) + \ddot{\psi}(t).\end{aligned} \tag{14}$$

Here, the controller gains K_c and K_p are positive. In PRERL, δ_0, α, p, q are controller tuning parameters to ensure the robustness and chattering mitigation [46].

Case I: Differential Braking Control (DBC) using PRERL

Using (14) and (4), the desired brake force control signal can now be obtained as,

$$\begin{aligned}F_i(t) = \frac{2}{d}\Bigg[\frac{-K_p}{\delta_0 + (1-\delta_0)e^{-\alpha|s(t)|^p}}\, |s(t)|^q\, \text{sgn}(s(t)) \\ + (-1)^{i+1}\, \lambda\dot{\psi}(t) \\ + (-1)^{i+1}\, \frac{l_f}{I_z}C_{\alpha f}\left(\frac{-v_y(t) + \dot{\psi}(t) l_f}{v_x(t)}\right) \\ + (-1)^{i}\, \frac{l_r}{I_z}C_{\alpha r}\left(\frac{-v_y(t) + \dot{\psi}(t) l_r}{v_x(t)}\right)\Bigg] \\ + (-1)^{2i}\, F_{(i+1)}(t) + (-1)^{2i+1}\, F_{(i+2)}(t) \\ + (-1)^{2i+2}\, F_{(i+3)}(t),\end{aligned} \tag{15}$$

where, $i = 0, 1, 2, 3$ and index of $F(t)$ is mod 4, implying a cyclic ordering of $F_0(t)$, $F_1(t)$, $F_2(t)$, and $F_3(t)$. Again, $F_0(t) = F_{xfl}(t)$, $F_1(t) = F_{xfr}(t)$, $F_2(t) = F_{xrl}(t)$, and $F_3(t) = F_{xrr}(t)$, represent the four longitudinal brake forces.

Here, (15) represents the control equation for DBC scheme, where the longitudinal forces are the control inputs.

Case II: Steering Angle Control (SAC) using PRERL

Using (14) and (4), the steering angle control signal $\delta(t)$ is obtained as,

$$\begin{aligned}\delta(t) = \frac{I_z}{l_f C_{\alpha f}}\Bigg[\frac{-K_p}{\delta_0 + (1-\delta_0)e^{-\alpha|s(t)|^p}}\, |s(t)|^q\, \text{sgn}(s(t)) \\ - \lambda\dot{\psi}(t)\Bigg] + \left(\frac{-v_y(t) + \dot{\psi}(t) l_f}{v_x(t)}\right) \\ + \frac{l_r C_{\alpha r}}{l_f C_{\alpha f}}\left(\frac{-v_y(t) + \dot{\psi}(t) l_r}{v_x(t)}\right) \\ + \frac{d}{2 l_f C_{\alpha f}}\left(F_{xfr}(t) - F_{xfl}(t)\right) \\ + \frac{d}{2 l_f C_{\alpha f}}\left(F_{xrr}(t) - F_{xrl}(t)\right).\end{aligned} \tag{16}$$

Equation (18) represents the control equation for SAC scheme, where the steering angle is the control input, and the four longitudinal forces used in the equation are obtained from the TruckMaker vehicle model.

Further, the performance of PRERL based DBC and SAC schemes has been compared with the conventional CRRL approach as given in case III and case IV.

This article has been accepted for publication in a future issue of this journal, but has not been fully edited. Content may change prior to final publication. Citation information: DOI 10.1109/ACCESS.2020.3024251, IEEE Access

Case III: Differential Braking Control (DBC) using CRRL

To obtain the control equations using CRRL, the reaching law given in (15) is replaced with that given in (13) to obtain

$$\begin{aligned} F_i(t) = \frac{2}{d}\Bigg[& -K_c \text{sgn}(s(t)) + (-1)^{i+1}\ \lambda\dot{\psi}(t) \\ & + (-1)^{i+1}\ \frac{l_f}{I_z} C_{\alpha f}\left(\frac{-v_y(t)+\dot{\psi}(t)l_f}{v_x(t)}\right) \\ & + (-1)^{i}\ \frac{l_r}{I_z} C_{\alpha r}\left(\frac{-v_y(t)+\dot{\psi}(t)l_r}{v_x(t)}\right)\Bigg] \\ & + (-1)^{2i}\ F_{(i+1)}(t) + (-1)^{2i+1}\ F_{(i+2)}(t) \\ & + (-1)^{2i+2}\ F_{(i+3)}(t). \end{aligned} \tag{17}$$

Case IV: Steering Angle Control (SAC) using CRRL

To obtain the control equations using CRRL, replace the reaching law given in (18) is replaced with that given in (13) to obtain

$$\begin{aligned} \delta(t) = & \frac{I_z}{l_f C_{\alpha f}}\left[-K_c \text{sgn}(s(t)) - \lambda\dot{\psi}(t)\right] \\ & + \left(\frac{-v_y(t)+\dot{\psi}(t)l_f}{v_x(t)}\right) \\ & + \frac{l_r C_{\alpha r}}{l_f C_{\alpha f}}\left(\frac{-v_y(t)+\dot{\psi}(t)l_r}{v_x(t)}\right) \\ & + \frac{d}{2 l_f C_{\alpha f}}\left(F_{xfr}(t) - F_{xfl}(t)\right) \\ & + \frac{d}{2 l_f C_{\alpha f}}\left(F_{xrr}(t) - F_{xrl}(t)\right). \end{aligned} \tag{18}$$

Controller parameters

The values of controller parameters are:

- DBC with PRERL law: The controller gain and tuning parameters are K_p = 3500, λ = 0.001, q = 0.4, δ_0 = 0.1, p = 1, α = 10.
- DBC with CRRL law: The controller gain and tuning parameter are K_c = 10, λ = 0.001.
- SAC with PRERL law: The controller gain and tuning parameters are K_p = 8300, λ = 1, q = 0.3, δ_0 = 0.8, p = 1, α = 10.
- SAC with CRRL law: The controller gain and tuning parameter are: K_c = 1000, λ = 1.

D. CONTROLLER IMPLEMENTATION

The controller design consists of two stages, namely the outer loop controller and the inner loop controller. The block diagram representation of the inner and outer loop controllers is given in Fig. 10. The outer loop consists of the vehicle's longitudinal speed and lateral speed estimation blocks that use a Sliding Mode Observer (SMO) design based on the information from the accelerometer and yaw rate sensors. The estimated longitudinal and lateral speeds are considered in the controller formulation. A fault identification block provides a fault flag, enabling the controller to provide the necessary control action. The longitudinal forces from the SMC were converted to the required brake chamber pressure and then converted to an equivalent Electro Pneumatic Regulator (EPR) voltage through an inner loop controller design based on Proportional Integral Derivative (PID) control. Also, a delay compensation technique was included to compensate for the delay effects in the air brake system [47]. Here, $y_d(t)$ is the desired pressure generated from the outer loop controller, $y(t)$ is the actual pressure value from the sensor, and $y_e(t)$ is the predicted pressure.

The SAC has been implemented through Software-in-the-Loop (SiL) platform. Here, the steering angle is the control input that is provided back to TruckMaker®.

E. STABILITY ANALYSIS

Lyapunov's stability analysis [44] was carried out for the PRERL based SMC with the selected sliding surface. Using (10), (11), and (12), $\dot{s}(t)$ can be written as,

$$\dot{s}(t) = \frac{-K_p}{\delta_0 + (1-\delta_0)e^{-\alpha|s(t)|^p}}\,|s(t)|^q\,\text{sgn}(s(t)) + b_d(t), \tag{19}$$

where b_d(t) represents the bounded disturbance in the system. The Lyapunov function for the above system was selected as

$$V(t) = \frac{1}{2}(s(t))^2. \tag{20}$$

Differentiating (20)

$$\dot{V}(t) = s(t)\dot{s}(t). \tag{21}$$

Substituting (19) in (21),

$$\dot{V}(t) = s(t)\left(\frac{-K_p}{\delta_0 + (1-\delta_0)e^{-\alpha|s(t)|^p}}\,|s(t)|^q\,\text{sgn}(s(t)) + b_d(t)\right). \tag{22}$$

Consider the magnitude of b_d(t) to be bounded by a positive scalar B and $\frac{K_p}{\delta_0+(1-\delta_0)e^{-\alpha|s(t)|^p}}\,|s(t)|^q = \rho$.

Equation (22) can now be written as,

$$\dot{V}(t) < |s(t)|B - s(t)\rho\text{sgn}(s(t)), \tag{23}$$

which can be rewritten as,

$$\dot{V}(t) < -|s(t)|(\rho - B). \tag{24}$$

For the asymptotic stability of the equilibrium point $(s(t)^* = 0)$, $\dot{V}(t) < 0, \forall s(t) \neq 0$. Hence,

$$|s(t)|(\rho - B) > 0 \Rightarrow \rho > B. \tag{25}$$

Hence, for asymptotic stability, the value of ρ should be chosen to be greater than that of B.

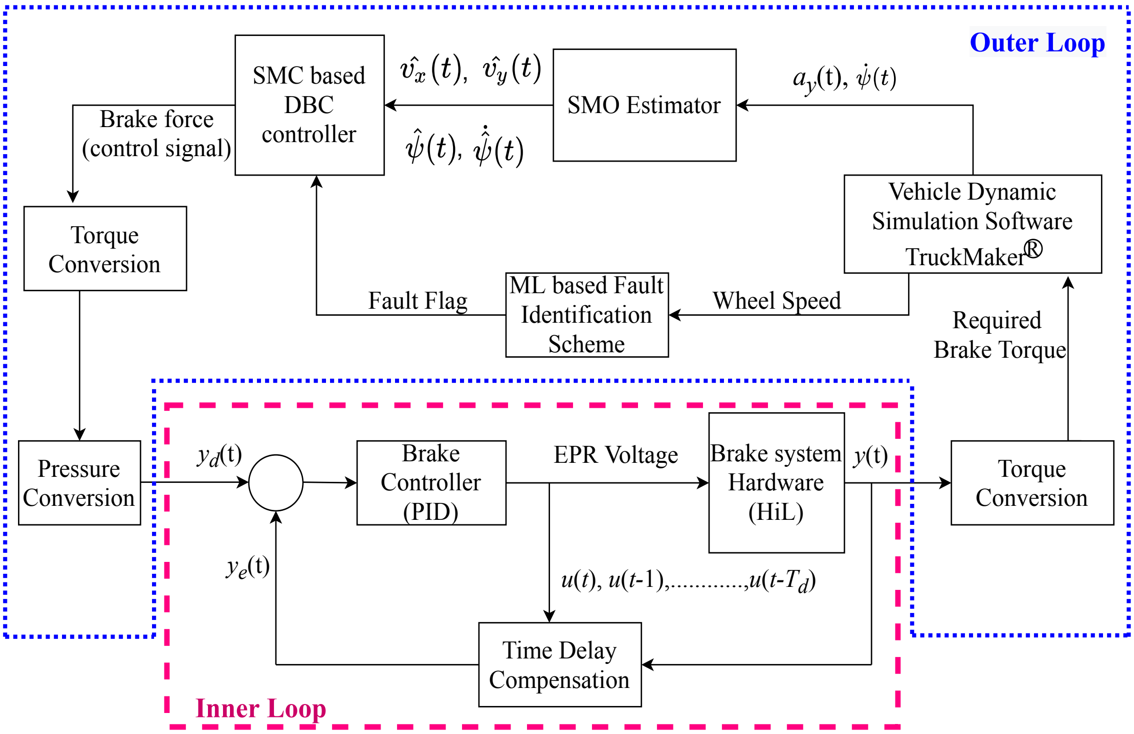

FIGURE 10: Inner and outer loop controller

F. PERFORMANCE ANALYSIS OF FTC

In this study, two control schemes, namely DBC and SAC, have been developed. Their performance has been analyzed based on the vehicle's yaw angle reduction and the stopping distance analysis. Both control schemes use the SMC technique with PRERL. The designed controller's performance has also been compared with the conventional SMC technique, which uses CRRL. The performance of the controllers was analyzed for various vehicle load (fully laden and fully unladen), road (tire-road friction coefficients, $\mu_{max} = 0.3$ and 0.8), and fault scenarios (20%, 50%, and 90% fault levels). Fig. 11 shows the brake torque, brake force, EPR voltage, steering angle, and yaw angle characteristics for a fully laden vehicle on a high-μ surface with 50% fault on the front right brake. With the presence of 50% fault on the front right brake, the brake torque and brake force on all four brakes without control action are shown in Fig. 11 (a) and (b), respectively. The same with the control action of CRRL based DBC are shown in Fig. 11 (c) and (e) and PRERL based DBC are shown in Fig. 11 (d) and (f). Fig. 11 (g) shows the equivalent EPR voltage corresponding to the control signal representing the front left brake force obtained through CRRL based DBC and PRERL based DBC. Fig. 11 (h) shows steering angle control signal obtained through CRRL based SAC and PRERL based SAC. In both cases, chattering introduced by the conventional CRRL approach has been mitigated by the PRERL based approach. Finally, Fig. 11 (i) and (j) show the corresponding yaw angle corrections. In order to select suitable control action with the presence of brake fault, an analysis based on yaw angle reduction and SD has been conducted, and the results are shown in Fig. 12 (a) and 12 (b). The performance of both DBC and SAC for various vehicle load, different fault levels (20%, 50% and 90% fault in the front right brake), with CRRL and PRERL reaching law and maximum tire-road friction coefficients (0.8 and 0.3) are quantified in Table 5. The performance of DBC and SAC schemes with CRRL and PRERL approaches under various vehicle operating scenarios are summarized below:

- **Scenario 1: Fully laden vehicle with $\mu_{max} = 0.8$ and 20% brake fault**. In this scenario, the yaw angle reduction of all the controllers (DBC with PRERL and CRRL and SAC with PRERL and CRRL) was above 95%. The increase in stopping distance was more than 5 m with the DBC scheme and less than 0.94 m with the SAC scheme.
- **Scenario 2: Fully laden vehicle with $\mu_{max} = 0.8$ with 50% brake fault.** The yaw angle reduction was 100% with the DBC scheme. SAC with PRERL and CRRL provided a yaw angle reduction of 97.46% and 96.16%, respectively. The increase in stopping distance corresponding to DBC with PRERL and CRRL was 11.59 m and 5.61 m, respectively, while that corresponding to SAC with PRERL and CRRL schemes was less than 0.91 m.
- **Scenario 3: Fully laden vehicle with $\mu_{max} = 0.8$ with 90% brake fault.** The yaw angle reduction was

This article has been accepted for publication in a future issue of this journal, but has not been fully edited. Content may change prior to final publication. Citation information: DOI 10.1109/ACCESS.2020.3024251, IEEE Access

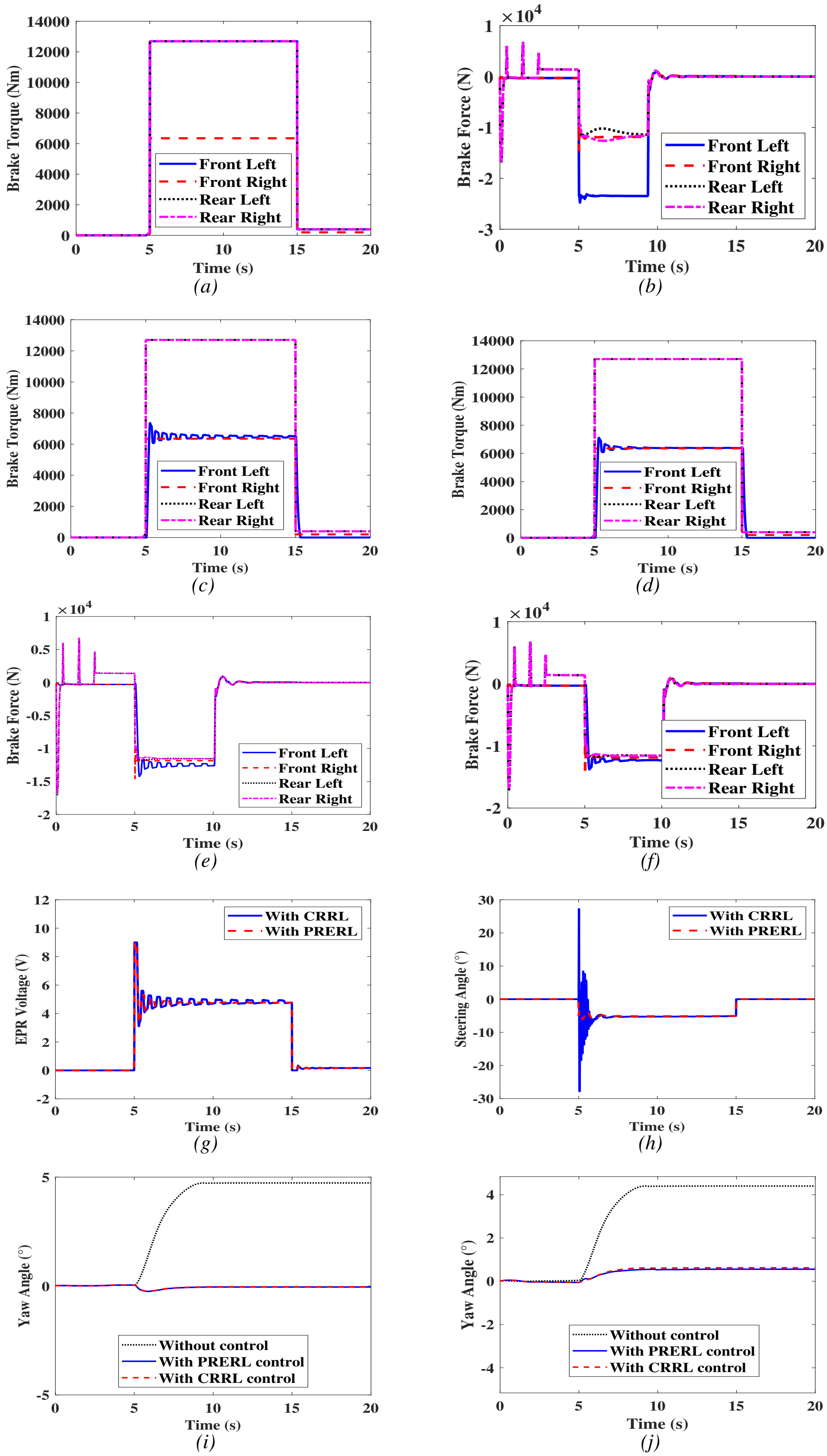

FIGURE 11: Fully laden vehicle performance characteristics in the presence of 50% brake fault on a dry road surface: a) Brake torque without control, b) Brake force without control, c) Brake torque with CRRL control, d) Brake torque with PRERL control, e) Brake force with CRRL control, f) Brake force with PRERL control, g) Equivalent EPR voltage corresponding to control signal, h) Steering angle control signal, i) Yaw angle without DBC and with PRERL based DBC and CRRL based DBC, j) Yaw angle without SAC and with PRERL based SAC and CRRL based SAC

This article has been accepted for publication in a future issue of this journal, but has not been fully edited. Content may change prior to final publication. Citation information: DOI 10.1109/ACCESS.2020.3024251, IEEE Access

TABLE 5: Performance analysis of FTC

Fully Laden Vehicle with $\mu_{max} = 0.8$					**Fully Laden Vehicle with $\mu_{max} = 0.3$**			**Fully Unladen Vehicle with $\mu_{max} = 0.8$**			**Fully Unladen Vehicle with $\mu_{max} = 0.3$**		
Fault level		**20 %**	**50%**	**90%**	**20 %**	**50%**	**90%**	**20 %**	**50%**	**90%**	**20 %**	**50%**	**90%**
Yaw Angle (^{o})	With Fault	1.82	4.72	9.26	1.03	2.65	4.711	4.49	11.89	28.6	1.12	2.64	4.72
	DBC (PRERL)	0.05	-0.03	0.004	-0.006	-0.002	-0.001	0.0172	0.011	0.08	0.016	0.05	0.013
	DBC (CRRL)	-0.93	-0.045	0.064	-0.0182	0.059	-0.0125	0.015	-0.45	0.05	0.156	0.042	0.122
	SAC (PRERL)	0.08	0.12	0.42	0.000006	0.003	0.002	0.08	0.15	0.05	0.04	0.002	0.002
	SAC (CRRL)	0.84	0.45	0.59	-0.03	-0.043	-0.005	-0.008	0.053	0.824	0.133	0.07	0.112
Stopping Distance (m)	With Fault	41.94	45.41	51.01	143	149	166	49.3	53.03	60.91	146.6	159.3	176.08
	DBC (PRERL)	47.52	57	66	158	159	182	54.31	57.9	74.38	157	164.25	185.1
	DBC (CRRL)	47.5	57.02	66.66	157.9	158.2	182.6	54.05	58.52	74.46	157.1	165.3	185.5
	SAC (PRERL)	42.11	45.42	51.06	143.4	150	166.7	50	53.8	60.98	146.7	159.5	177
	SAC (CRRL)	41.9	46	51	144	150.5	166.68	49.5	54	61	146.74	159.4	176.2

99% with the DBC scheme (both PRERL and CRRL), while the corresponding value for the SAC scheme (both PRERL and CRRL) was 95%. The increase in stopping distance corresponding to DBC with PRERL and CRRL was 14.99 m and 16.99 m, respectively, while that corresponding to SAC with PRERL and CRRL schemes was less than 0.09 m.

- **Scenario 4: Fully laden vehicle with $\mu_{max} = 0.3$ with 20% brake fault.** The yaw angle reduction with all controllers (DBC with PRERL and CRRL and SAC with PRERL and CRRL) was 100%. The increase in stopping distance corresponding to DBC with PRERL and CRRL was 15 m and 14.90 m, respectively, while that corresponding to SAC with PRERL and CRRL schemes was less than 0.4 m.
- **Scenario 5: Fully laden vehicle with $\mu_{max} = 0.3$ with 50% brake fault.** The yaw angle reduction with DBC scheme (both PRERL and CRRL) and SAC scheme (both PRERL and CRRL) was higher than 97.77% and 95%, respectively. The increase in stopping distance corresponding to DBC with PRERL and CRRL was 10 m and 8 m, respectively, while that corresponding to SAC with PRERL, and the CRRL scheme was less than 1 m.
- **Scenario 6: Fully laden vehicle with $\mu_{max} = 0.3$ with 90% brake fault.** The yaw angle reduction with all controllers (DBC with PRERL and CRRL and SAC with PRERL and CRRL) was 100%. The increase in stopping distance corresponding to DBC with PRERL and CRRL was 16 m and 15 m, respectively, while that corresponding to SAC with PRERL and CRRL scheme was less than 0.7 m.
- **Scenario 7: Fully Unladen vehicle with $\mu_{max} = 0.8$ with 20% brake fault.** The yaw angle reduction with DBC scheme (both PRERL and CRRL) and SAC scheme (both PRERL and CRRL) was higher than 99.67% and 98.22%, respectively. The increase in stopping distance corresponding to DBC with PRERL and CRRL was 5.01 m and 4.75 m, respectively, while that corresponding to SAC with PRERL and CRRL scheme was less than 1.7 m.
- **Scenario 8: Fully Unladen vehicle with $\mu_{max} = 0.8$ with 50% brake fault.** The yaw angle reduction with the DBC scheme (both PRERL and CRRL) and with the SAC scheme (both PRERL and CRRL) was higher than 99.91% and 98.74%, respectively. The increase in stopping distance corresponding to DBC with PRERL and CRRL was 4.87 m and 5.49 m, respectively, while that corresponding to SAC with PRERL and CRRL

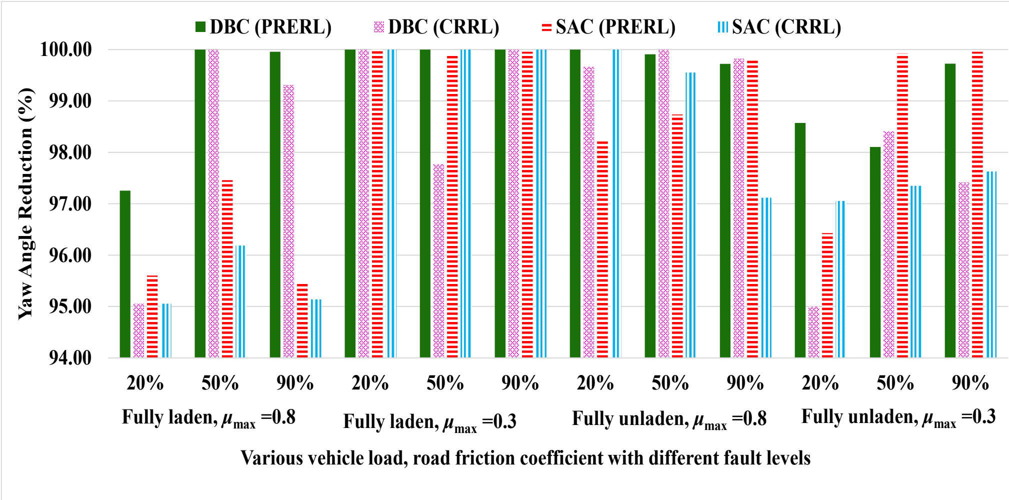

(a)

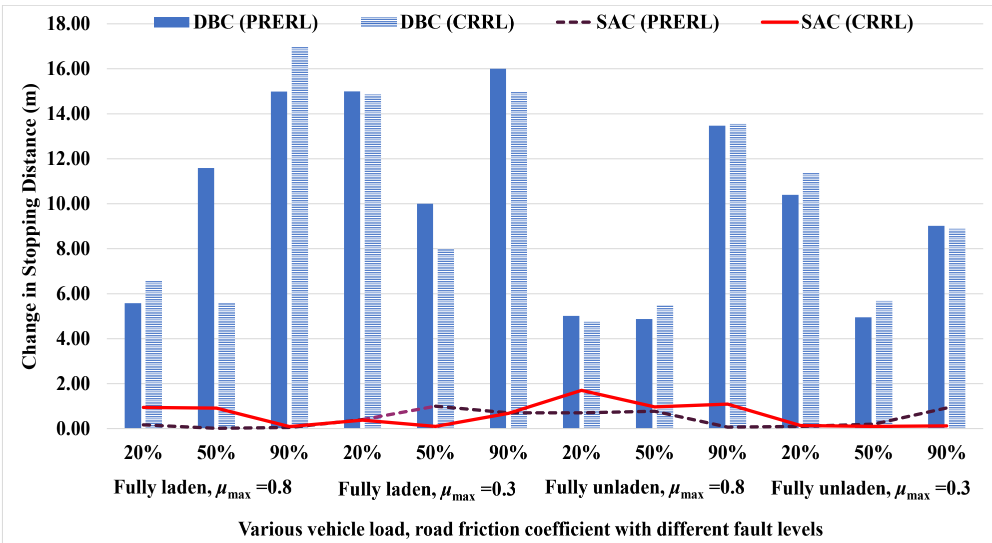

(b)

FIGURE 12: Performance comparison of DBC and SAC based on a) Yaw Angle Reduction and b) Stopping Distance

scheme was less than 0.97 m.

- **Scenario 9: Fully Unladen vehicle with** $\mu_{max} = 0.8$ **with 90% brake fault.** The yaw angle reduction with the DBC scheme (both PRERL and CRRL) and with the SAC scheme (both PRERL and CRRL) was greater than 99.72% and 97.12%, respectively. The increase in stopping distance corresponding to DBC with PRERL and CRRL was 13.47 m and 13.49 m, respectively, while that corresponding to SAC with PRERL and CRRL scheme was less than 1.09 m.
- **Scenario 10: Fully Unladen vehicle with** $\mu_{max} = 0.3$ **with 20% brake fault.** The yaw angle reduction with the DBC scheme (both PRERL and CRRL) and with the SAC scheme (both PRERL and CRRL) was greater than 95% and 96.43%, respectively. The increase in stopping distance corresponding to DBC with PRERL and CRRL was 10.40 m and 11.40 m, respectively, while that corresponding to SAC with PRERL and CRRL scheme was less than 0.14 m.
- **Scenario 11: Fully Unladen vehicle with** $\mu_{max} = 0.3$ **with 50% brake fault.** The yaw angle reduction with the DBC scheme (both PRERL and CRRL) and with the SAC scheme (both PRERL and CRRL) was 98% and greater than 97.35%, respectively. The increase in stopping distance corresponding to DBC with PRERL and CRRL was 4.95 m and 5.70 m, respectively, while that corresponding to SAC with PRERL and CRRL scheme was less than 0.2 m.

This article has been accepted for publication in a future issue of this journal, but has not been fully edited. Content may change prior to final publication. Citation information: DOI 10.1109/ACCESS.2020.3024251, IEEE Access

- **Scenario 12: Fully Unladen vehicle with $\mu_{max} = 0.3$ with 90% brake fault.** The yaw angle reduction with the DBC scheme (both PRERL and CRRL) and with the SAC scheme (both PRERL and CRRL) was greater than 97.42% and 97.63%, respectively. The increase in stopping distance corresponding to DBC with PRERL and CRRL was 9.02 m and 8.92 m, respectively, while that corresponding to SAC with PRERL and CRRL scheme was less than 0.92 m.

From this analysis, it is clear that both the DBC and the SAC controllers gave good tracking accuracy (greater than 95%) as shown in Fig. 12 (a). However, DBC results in an increase of SD to maintain directional stability. This is due to the reduction in the net brake force occurring as a result of DBC trying to balance the brake torque on both sides of the vehicle, as shown in Fig. 11 (a) and (c). The CRRL scheme's disadvantage is the high chattering in the control signal, as shown in Fig. 11 (g) and (h). By analyzing the above twelve scenarios, it was concluded that the SAC with the PRERL scheme provided better control action with a lower increase in stopping distance in the presence of brake faults. Even though the SAC provides appreciably good tracking accuracy along with a lower increase in stopping distance, there exists a trade-off between the DBC and SAC in view of their practical implementation. Given the active braking control systems already present in production vehicles, DBC is easier to implement practically. In the case of SAC, the corresponding controller needs to apply the steering angle control input through the steering system and this would be felt by the driver. This may lead to potential conflict with the driver's steering command and lead to non-acceptance by drivers. However, since SAC provides better performance in terms of a lower increase in SD, it is a good candidate for implementation in autonomous vehicles.

G. ROBUSTNESS ANALYSIS

The robustness of the controller has been evaluated by testing the controller performance under a side wind disturbance. The vehicle under study is a fully laden vehicle in a straight line maneuver on a road with a maximum friction coefficient of 0.8. The side wind force used in this study is shown in Fig. 13 (a), which consists of a ramp, step, and sinusoidal signals [48]. It can be seen from Fig. 13 (b) that while the side wind force further increased the yaw angle in the absence of control, the controller was able to reduce the same and maintain the straight-line trajectory. Since the SAC scheme provided better control action with the faulty brakes, the robustness analysis was done for the SAC scheme. It was observed that the SAC with the CRRL scheme provided 90.2% yaw angle reduction, while the SAC with the PRERL scheme shows better control action with 94.3% yaw angle reduction.

In the case of heavy commercial road vehicles, vehicle mass highly depends on the vehicle's load condition. For the considered class of vehicles, mass is different for fully laden (16200 kg) and unladen (4700 kg) vehicle. Moreover,

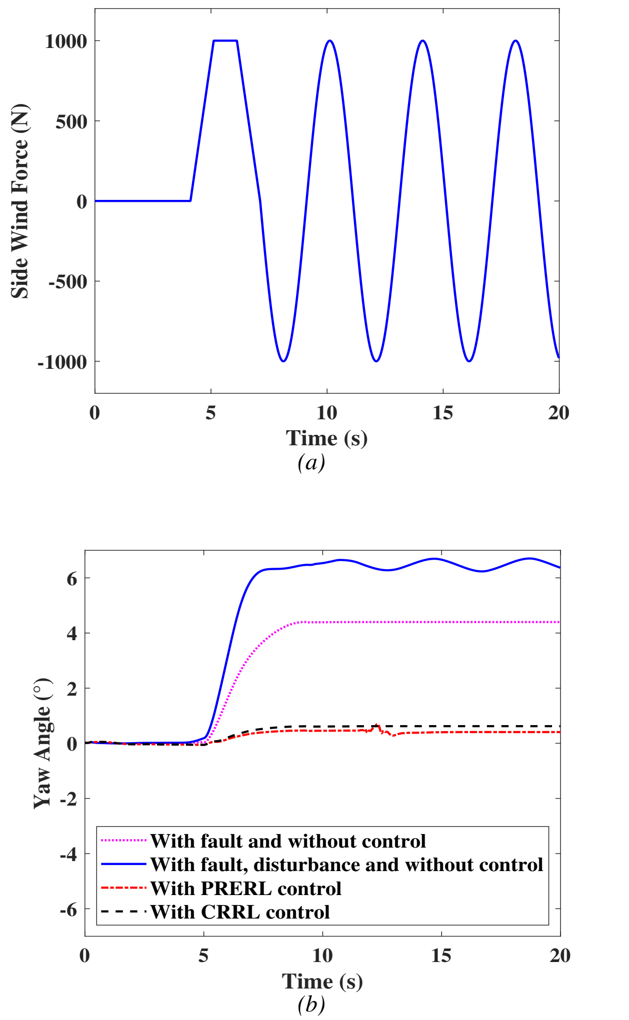

FIGURE 13: Robustness analysis: a) Side wind force disturbance input and b) Yaw angle with and without SAC scheme when the vehicle under side wind force disturbance

for fully laden and unladen vehicles, the moment of inertia (z-axis) and CG height are different. Also, the total force-generating capacity of a tire-road interaction decreases from a high friction surface (dry) to a low friction surface (snowy). Hence, in the lateral motion, the lateral force saturation point is reached at a lower slip angle on a low friction surface compared to the dry friction surface. Also, the maximum longitudinal force is reduced from dry to snowy road surfaces. With different brake fault levels, the longitudinal forces also vary. A fixed controller parameter set that provides good performance in the presence of these parametric uncertainties was obtained. The controller gave a robust performance in various vehicle operating scenarios such as fully laden and unladen conditions, operation on different road surfaces (dry and snowy), and different fault levels (20%, 50%, and 90%).

This article has been accepted for publication in a future issue of this journal, but has not been fully edited. Content may change prior to final publication. Citation information: DOI 10.1109/ACCESS.2020.3024251, IEEE Access

VII. CONCLUSION

This paper primarily focused on designing a fault identification scheme and a fault-tolerant control scheme for an air brake system to improve the directional stability of HCRVs under brake fault scenarios. A multiclass classification algorithm has been developed to identify the various levels of faults. Further, an FTC algorithm using SMC (both DBC and SAC) was designed and analyzed for its performance in containing the adverse effects of faulty brake on vehicle stability.

The main highlights of the paper are:

- Six multiclass ML models were developed and trained using data sets collected from 1296 experimental test cases and tested with 499 data sets.
- The Random Forest model gave better classification accuracy of 91.99 % compared to other ML models.
- The designed FTC with DBC was evaluated in HiL experimental setup and SAC with SiL experimental setup.
- The design of DBC and SAC schemes used two reaching laws, namely PRERL and CRRL. On comparing the FTC scheme based on the reaching laws, the PRERL based SAC scheme provided better tracking accuracy.
- For a 50 % torque reduction on the front right brake of a fully laden vehicle with 0.8 tire-road friction coefficient, SAC-based FTC gave better tracking accuracy of 97.46 % (yaw angle) with a very small increase in SD (0.01 m) compared to DBC-based FTC .

In the current study, all the test scenarios were evaluated in a HiL platform with the air brake hardware and TruckMaker® software. Implementation of the developed algorithms for on-road vehicles can be considered as future scope.

REFERENCES

[1] S. C. Subramanian, S. Darbha, and K. Rajagopal, "A diagnostic system for air brakes in commercial vehicles," *IEEE Transactions on Intelligent Transportation systems*, vol. 7, no. 3, pp. 360–376, 2006.

[2] L. Kandt, P. Reinhall, and R. Scheibe, "Determination of air brake adjustment from air pressure data," *Proceedings of the Institution of Mechanical Engineers, Part D: Journal of Automobile Engineering*, vol. 215, no. 1, pp. 21–29, 2001.

[3] S. Dhar, *Development of diagnostic algorithms for air brakes in trucks*. Texas A&M University, 2010.

[4] National Highway Traffic Safety Administration (NHTSA), Department of Transportation , *Federal Motor Vehicle Safety Standard-49 CFR Part 571.121 (FMVSS 121), Air brake systems*, U.S.A.,2018.

[5] National Transport Commission , *Report on National Heavy Vehicle Braking Strategy*, November, 2008.

[6] Ministry of Road Transport & Highways, Transport Research Wing, *Road Transport Year Book 2015-2016*, New Delhi, India, 2018.

[7] J. C. de Souza Silva and J. C. H. Gutierrez, "Brake system regulation in brazil: An update about resolutions and statistics related to the theme and the scenario for esc," *13^{th} SAE Brazil International Brake Colloquium and Engineering Display*, 2017.

[8] L. H. Sepulvene, I. N. Drummond, B. T. Kuehne, R. M. Frinhani, F. Petri, S. Reiff-Marganiec, and B. G. Batista, "Analysis of machine learning techniques in fault diagnosis of vehicle fleet tracking modules," in *2019 8^{th} Brazilian Conference on Intelligent Systems (BRACIS)*, pp. 759–764, 2019.

[9] X. Tang and A. Xu, "Multi-class classification using kernel density estimation on k-nearest neighbours," *Electronics Letters*, vol. 52, no. 8, pp. 600–602, 2016.

[10] C. Sankavaram, B. Pattipati, K. Pattipati, Y. Zhang, M. Howell, and M. Salman, "Data-driven fault diagnosis in a hybrid electric vehicle regenerative braking system," in *2012 IEEE Aerospace Conference*. IEEE, 2012, pp. 1–11.

[11] L. Huang, Q. Zeng, and R. Zhang, "Fuel cell engine fault diagnosis expert system based on decision tree," in *2019 IEEE 3rd Information Technology, Networking, Electronic and Automation Control Conference (ITNEC)*. IEEE, 2019, pp. 282–286.

[12] J. J. Rodriguez, L. I. Kuncheva, and C. J. Alonso, "Rotation forest: A new classifier ensemble method," *IEEE Transactions on Pattern Analysis and Machine Intelligence*, vol. 28, no. 10, pp. 1619–1630, 2006.

[13] Q. Yao, J. Wang, L. Yang, H. Su, and G. Zhang, "A fault diagnosis method of engine rotor based on random forests," in *2016 IEEE International Conference on Prognostics and Health Management (ICPHM)*. IEEE, 2016, pp. 1–4.

[14] S. Kaplan, M. A. Guvensan, A. G. Yavuz, and Y. Karalurt, "Driver behavior analysis for safe driving: A survey," *IEEE Transactions on Intelligent Transportation Systems*, vol. 16, no. 6, pp. 3017–3032, 2015.

[15] J. M. Choi, S.-Y. Liu, and J. K. Hedrick, "Human driver model and sliding mode control-road tracking capability of the vehicle model," in *2015 European Control Conference (ECC)*. IEEE, 2015, pp. 2132–2137.

[16] L. Saleh, P. Chevrel, F. Mars, J.-F. Lafay, and F. Claveau, "Human-like cybernetic driver model for lane keeping," *IFAC Proceedings Volumes*, vol. 44, no. 1, pp. 4368–4373, 2011.

[17] C. K. Song, M. Uchanski, and J. K. Hedrick, "Vehicle speed estimation using accelerometer and wheel speed measurements," SAE Technical Paper, Tech. Rep., 2002.

[18] L. Chu, Y. Shi, Y. Zhang, H. Liu, and M. Xu, "Vehicle lateral and longitudinal velocity estimation based on adaptive kalman filter," in *2010 3rd International Conference on Advanced Computer Theory and Engineering (ICACTE)*, vol. 3. IEEE, 2010, pp. V3–325.

[19] Y. Zhang, Z. Zhao, T. Lu, L. Yuan, W. Xu, and J. Zhu, "A comparative study of luenberger observer, sliding mode observer and extended kalman filter for sensorless vector control of induction motor drives," in *2009 IEEE Energy Conversion Congress and Exposition*. IEEE, 2009, pp. 2466–2473.

[20] H. Shraim, M. Ouladsine, L. Fridman, and M. Romero, "Vehicle parameter estimation and stability enhancement using sliding modes techniques," *International Journal of Vehicle Design*, vol. 48, no. 3-4, pp. 230–254, 2008.

[21] Y. Chen, Y. Ji, and K. Guo, "A reduced-order nonlinear sliding mode observer for vehicle slip angle and tyre forces," *Vehicle System Dynamics*, vol. 52, no. 12, pp. 1716–1728, 2014.

[22] H. Li, H. Liu, H. Gao, and P. Shi, "Reliable fuzzy control for active suspension systems with actuator delay and fault," *IEEE Transactions on Fuzzy Systems*, vol. 20, no. 2, pp. 342–357, 2011.

[23] C. Huang, F. Naghdy, and H. Du, "Observer-based fault-tolerant controller for uncertain steer-by-wire systems using the delta operator," *IEEE/ASME Transactions on Mechatronics*, vol. 23, no. 6, pp. 2587–2598, 2018.

[24] T. Youssef and M. Chadli, "Observer-based fault tolerant tracking control for ts fuzzy models subject to actuator faults," *IFAC-PapersOnLine*, vol. 48, no. 21, pp. 1024–1029, 2015.

[25] F. Chen, J. Niu, and G. Jiang, "Nonlinear fault-tolerant control for hypersonic flight vehicle with multi-sensor faults," *IEEE Access*, vol. 6, pp. 25 427–25 436, 2018.

[26] B. Guo and Y. Chen, "Output integral sliding mode fault tolerant control for nonlinear systems with actuator fault and mismatched disturbance," *IEEE Access*, vol. 6, pp. 59 383–59 393, 2018.

[27] R. Kazemi and A. Janbakhsh, "Nonlinear adaptive sliding mode control for vehicle handling improvement via steer-by-wire," *International Journal of Automotive Technology*, vol. 11, no. 3, pp. 345–354, 2010.

[28] H. Zhou and Z. Liu, "Vehicle yaw stability-control system design based on sliding mode and backstepping control approach," *IEEE Transactions on Vehicular Technology*, vol. 59, no. 7, pp. 3674–3678, 2010.

[29] R. G. Hebden, C. Edwards, and S. K. Spurgeon, "An application of sliding mode control to vehicle steering in a split-mu maneuver," in *Proceedings of the 2003 American Control Conference, 2003.*, vol. 5. IEEE, 2003, pp. 4359–4364.

[30] M. Chae, Y. Hyun, K. Yi, and K. Nam, "Dynamic handling characteristics control of an in-wheel-motor driven electric vehicle based on multiple sliding mode control approach," *IEEE Access*, vol. 7, pp. 132 448–132 458, 2019.

This article has been accepted for publication in a future issue of this journal, but has not been fully edited. Content may change prior to final publication. Citation information: DOI 10.1109/ACCESS.2020.3024251, IEEE Access

[31] R. Liu, Z. Sun, and D. Ye, "Adaptive sliding mode control for spacecraft autonomous rendezvous with elliptical orbits and thruster faults," *IEEE Access*, vol. 5, pp. 24 853–24 862, 2017.
[32] G. M. Anche, K. Devika, and S. C. Subramanian, "Robust pitching disturbance force attenuation for tractor considering functional constraints," *IEEE Access*, vol. 8, pp. 86 419–86 432, 2020.
[33] J. Y. Hung, W. Gao, and J. C. Hung, "Variable structure control: A survey," *IEEE Transactions on Industrial Electronics*, vol. 40, no. 1, pp. 2–22, 1993.
[34] D. M. Farid, N. Harbi, and M. Z. Rahman, "Combining naive bayes and decision tree for adaptive intrusion detection," *International Journal of Network Security & Its Applications (IJNSA), Vol. 2, pp. 12-25, 2010*.
[35] J. R. Quinlan, "Induction of decision trees," *Machine Learning*, vol. 1, no. 1, pp. 81–106, 1986.
[36] L. Breiman, "Random forests," *Machine Learning*, vol. 45, no. 1, pp. 5–32, 2001.
[37] R. Jegadeeshwaran and V. Sugumaran, "Fault diagnosis of automobile hydraulic brake system using statistical features and support vector machines," *Mechanical Systems and Signal Processing*, vol. 52, pp. 436–446, 2015.
[38] R. Rifkin and A. Klautau, "In defense of one-vs-all classification," *Journal of Machine Learning Research*, vol. 5, no. Jan, pp. 101–141, 2004.
[39] A. Widodo and B.-S. Yang, "Support vector machine in machine condition monitoring and fault diagnosis," *Mechanical Systems and Signal Processing*, vol. 21, no. 6, pp. 2560–2574, 2007.
[40] A. L. (2017). Comet 1612il. [Online]. Available: https://trucks.cardekho.com/ en/trucks/ashok-leyland/1616-il
[41] A. L. Dunn, D. A. Guenther, and R. Radlinski, "Application of air brake performance relationships in accident reconstruction and their correlation to real vehicle performance," *SAE International Journal of Commercial Vehicles*, vol. 5, no. 2012-01-0609, pp. 251–270, 2012.
[42] H. Pacejka, *Tire and vehicle dynamics*. Elsevier, 2005.
[43] IPG Automotive GmbH, "IPG TruckMaker® Reference Manual Version 6.0.5," 2017.
[44] J.-J. E. Slotine, "Sliding controller design for non-linear systems," *International Journal of control*, vol. 40, no. 2, pp. 421–434, 1984.
[45] W. Wang, J. Yi, D. Zhao, and D. Liu, "Design of a stable sliding-mode controller for a class of second-order underactuated systems," *IEE Proceedings-Control Theory and Applications*, vol. 151, no. 6, pp. 683–690, 2004.
[46] K. Devika and S. Thomas, "Power rate exponential reaching law for enhanced performance of sliding mode control," *International Journal of Control, Automation and Systems*, vol. 15, no. 6, pp. 2636–2645, 2017.
[47] N. Sridhar, K. Devika, S. C. Subramanian, G. Vivekanandan, and S. Sivaram, "Antilock brake algorithm for heavy commercial road vehicles with delay compensation and chattering mitigation," *Vehicle System Dynamics*, pp. 1–21, 2019.
[48] X. Diao, Y. Jin, L. Ma, S. Ding, and H. Jiang, "Composite active front steering controller design for vehicle system," *IEEE Access*, vol. 5, pp. 6697–6706, 2017.

RADHIKA RAVEENDRAN received her bachelor's degree in electrical and electronics engineering from Mahatma Gandhi University, and Master's degree in guidance, navigation and control from University of Kerala. She is currently pursuing Ph. D. in vehicle dynamics and control in the Department of Engineering Design at IIT Madras, Chennai, India. Her research interests include, control of automotive systems, fault prognosis and condition monitoring of electro-mechanical systems.

K. B. DEVIKA received the bachelor's degree in electrical and electronics engineering from Mahatma Gandhi University, the master's degree in guidance, navigation and control from the University of Kerala, and the Ph.D. degree in control systems from the National Institute of Technology, Calicut. She is currently a Post-Doctoral Fellow at the Department of Engineering Design, IIT Madras, India. Her research interests include control of automotive and aerospace systems and sliding mode control.

SHANKAR C. SUBRAMANIAN (Senior Member, IEEE) received the B.E. degree in mechanical engineering from Motilal Nehru Regional Engineering College, Allahabad, India, and the M.S. and Ph.D. degrees from Texas A&M University, USA. He is currently a Professor and a V. Ramamurti Faculty Fellow with the Department of Engineering Design, IIT Madras, Chennai, India. His research interests include dynamics and control with applications to automotive and transportation systems.

• • •